SCIENCE CHINA
Information Sciences

• RESEARCH PAPER •

May 2023, Vol. 66 152205:1–152205:19
https://doi.org/10.1007/s11432-022-3647-7

Variable-order fractional derivative rutting depth prediction of asphalt pavement based on the RIOHTrack full-scale track

Yu WANG[1,2], Jiaojiao YAN[1,2], Wei HUANG[3], Leszek RUTKOWSKI[4,5,6] & Jinde CAO[1,2,7*]

[1]*School of Mathematics, Southeast University, Nanjing* 210096*, China;*
[2]*Jiangsu Provincial Key Laboratory of Networked Collective Intelligence, Southeast University, Nanjing* 210096*, China;*
[3]*Intelligent Transportation System Research Center, Southeast University, Nanjing* 210096*, China;*
[4]*Systems Research Institute of the Polish Academy of Sciences, Warsaw* 01-447*, Poland;*
[5]*Institute of Computer Science, AGH University of Science and Technology, Krakow* 30-059*, Poland;*
[6]*Information Technology Institute, University of Social Sciences, Lodz* 90-113*, Poland;*
[7]*Yonsei Frontier Lab, Yonsei University, Seoul* 03722*, Republic of Korea*

Received 28 June 2022/Revised 6 September 2022/Accepted 11 November 2022/Published online 21 April 2023

Abstract Rutting deformation is typical damage to asphalt pavement and can be quantitatively described as the time-varying mechanical deformation feature of the asphalt mixture during the creep process. First, a nonlinear viscoelastic creep model is established based on the Caputo variable-order fractional derivative. The fractional order in this model is not fixed and is defined as a time-varying function. The time-dependent mechanical properties of asphalt mixtures are effectively reflected. Based on the modified Burgers model, the variable-order function is revised to a linear form. Second, the variable-order fractional Burgers rutting model is obtained by fitting the test data of the RIOHTrack full-scale track. The Levenberg-Marquardt optimization algorithm is used to analyze the test data and the corresponding parameters to obtain more accurate and applicable variable-order fractional rutting mechanics and empirical models for different asphalt pavement structures. Finally, according to the classification of the pavement structure, structures III and VI are taken as examples. The rutting prediction and comparison results of several representative pavement structures are obtained to verify that the proposed rutting prediction model can also accurately predict all road sections of RIOHTrack. The new model is also compared with the rutting model of the mechanistic-empirical pavement design guide, the fractional-order Burgers rutting model, and the modified Burgers rutting model. The fitting results are evaluated using the determination coefficient R^2. The results show that the variable-order fractional Burgers rutting model proposed in this study exhibits a better fit and is more applicable to describe the rutting deformation of asphalt pavement.

Keywords RIOHTrack full-scale track, Caputo fractional derivative, variable-order fractional, modified Burgers model, rutting prediction

Citation Wang Y, Yan J J, Huang W, et al. Variable-order fractional derivative rutting depth prediction of asphalt pavement based on the RIOHTrack full-scale track. Sci China Inf Sci, 2023, 66(5): 152205, https://doi.org/10.1007/s11432-022-3647-7

1 Introduction

Asphalt pavement has been widely used in highway construction because of its advantages of smoothness, less dust, short construction period, and durability [1]. However, with the significant increase in traffic volume and axle load, the damage to asphalt pavement will become more obvious. Among them, rutting is one of the main pavement diseases formed after pavement damage. In severe cases, deformation will occur on both sides of the rut, resulting in serious deterioration of pavement performance [2–4]. Creep is one of the most important mechanical properties of asphalt mixtures, which is directly related to rutting behavior [5]. By establishing a reasonable creep model of asphalt mixture, a prediction model that is

* Corresponding author (email: jdcao@seu.edu.cn)

more suitable for rutting depth, which is of great significance for road rutting detection and prediction, can be obtained through further calculations and can provide important information for the structural design and maintenance of asphalt pavements.

In recent years, researchers have proposed many asphalt pavement rutting prediction models, which are mainly divided into three categories, that is, empirical, mechanical, and mechanical-empirical models. Among them, the empirical model is calibrated on the field test rutting depth data and subjected to strict field test conditions [6, 7]. The mechanical model is a rutting prediction model established based on the viscoelastic-plastic material mechanics theory, which is the most rigorous model. However, its establishment process requires a series of assumptions, which cannot fully consider the actual road performance, and there may be a large error between actual and predicted rutting depths [8–11]. Moreover, with the development of artificial intelligence and machine learning technology, researchers began to use neural networks and deep learning methods to predict the depth of road rutting [12–16]. Models based on neural network technology have considerable predictive capabilities, but they only predict future rutting depths by training on laboratory and field test data. Furthermore, the mechanical properties of asphalt pavement materials cannot be fully considered, the mechanical explanation of the evolutionary process of pavement rutting is lacking, and a clear expression that can be used for the rutting prediction cannot be obtained.

The mechanical-empirical model is an empirical theoretical model established by analyzing the stress-strain response of the pavement structure based on the viscoelastic-plastic layered system theory and corrected based on the relevant data of the test section. This model combines the advantages of mechanical and empirical models [5, 17–21]. Thus far, many mechanical-empirical differential constitutive models have been proposed to investigate the dynamic viscoelastic behavior of asphalt mixtures [5, 22]. Among them, classical differential constitutive models, such as the Kelvin, Maxwell, and Burgers models, have been constructed using a series or parallel combination of a series of springs and stick pot elements. The differential operator in the aforementioned models is a local integer differential, but research shows that the fractional differential operator is more suitable for describing the memory properties of viscoelastic materials and constitutive equations of materials [23–25]. Then, with the continuous expansion of the asphalt engineering scale and the continuous improvement of the performance requirements of asphalt pavements, many scholars have begun to pay attention to research on the rheological properties of asphalt mixtures. The mechanical properties of asphalt mixtures are strongly time-dependent, which will become more obvious under the action of long-term time series and continuous load [26–28]. The aforementioned fractional differential constitutive model has limitations because the change in rheological properties during creep cannot be simulated if the fractional differentiation order is constant. Therefore, the variable-order fractional differential needs to be further considered in constructing the asphalt pavement constitutive model.

Variable-order fractional creep models have been widely used to analyze rocks, glass polymers, and some concrete materials. For example, Ref. [27] proposed a rock Maxwell creep model based on variable-order fractional derivatives, which use variable-order fractional components to represent the viscoelastic response and describe the viscoplastic response of plastic sliding bodies. The variable-order fractional differential full-scale rock creep model is proposed in [29], which verified that it can describe the three-model creep behavior of rock. This model has the advantage of a simple form and few parameters. However, for the constitutive model of asphalt pavement, only a few research results based on the variable-order fractional differential have been obtained. In [5], a nonlinear viscoelastic-plastic creep model based on the variable-order fractional calculus is proposed to quantitatively describe the time-varying mechanical properties of asphalt mixtures. The differential order of the variable-order fractional element of the model is a piecewise function, which reflects the different mechanical properties of the material in the viscoelastic and viscoplastic stages. The test data used in this study come from a full-length track called RIOHTrack built in Beijing, China, which has multiple sets of pavement structures with different base types and measures and collects a large amount of reliable field data, such as environmental, material, and pavement service data [30, 31], ensuring convenience for the comparative study of model applicability of different types of asphalt pavement structures. At present, only a few conclusions about the rutting prediction mechanics empirical model of this track have been drawn. In [21], the authors established a pavement rutting prediction model based on different base types of asphalt in the RIOHTrack full-scale track and Burgers model.

Based on the previously presented discussion, to better reflect the mechanical rheological properties of asphalt mixtures, a variable-order fractional Burgers rutting depth prediction model is proposed in this

study. According to the rutting test data of RIOHTrack, the Levenberg-Marquardt (LM) algorithm is used to analyze the test data and fit the corresponding parameters to establish a more accurate and applicable mechanical-empirical model for different asphalt pavement structures. The paper is organized as follows: Section 2 provides the preliminaries that can be used in subsequent sections, including concepts, related conclusion, and proofs of the Caputo variable-order fractional differentiation and Laplace transforms. Section 3 sorts out the building process of the variable-order fractional Burgers rutting depth prediction model. Section 4 presents the pavement structures and the source and analysis of the dataset. Section 5 introduces the data fitting results of the developed depth prediction model and compares the fitting effect of this model with other rutting depth prediction models. Section 6 provides the conclusion of this study.

2 Preliminaries

2.1 Caputo fractional derivative

Compared with the Riemann-Liouville fractional differential, the initial value condition of the Caputo fractional differential has a clear physical meaning. Therefore, the fractional model in practical engineering is generally described as the Caputo fractional differential equation [32], which is defined as follows.

Definition 1 (Eq. (5) in [33]). The Caputo fractional differential of function $f(t)$ is expressed as follows:

$$ {}_{t_0}^{C}\mathscr{D}_t^{\alpha} f(t) = \frac{1}{\Gamma(n-\alpha)} \int_{t_0}^{t} \frac{f^{(n)}(\tau)}{(t-\tau)^{\alpha-n+1}}\, \mathrm{d}\tau, \quad n = \lceil \alpha \rceil, \tag{1} $$

where ${}_{t_0}^{C}\mathscr{D}_t^{\alpha} f(t)$ is the fractional differential operator, C is the Caputo fractional differential, $n-1 < \alpha < n$ is the fractional order, $\lceil \cdot \rceil$ is the roundup function, and t and t_0 are the upper and lower limits of the integral, respectively. $\Gamma(\cdot)$ is the Gamma function, which is defined as follows:

$$ \Gamma(z) = \int_0^{\infty} \mathrm{e}^{-t} t^{z-1}\, \mathrm{d}t, \ \mathrm{Re}(z) > 0. \tag{2} $$

To determine the commutative law of the Caputo fractional differentiation with more general conditions, we know that the following commutative law computation of fractional integrals is reasonable in advance.

Lemma 1 (Theorem 2.2 of [34]). Let $m, n \geqslant 0$ and $f(t) \in L_1[t_0, t]$; that is, $f(t)$ is a Lebesgue integrable function. Then, $J_{t_0}^{m} J_{t_0}^{n} f(t) = J_{t_0}^{m+n} f(t)$ holds nearly everywhere on $[t_0, t]$, where $J_{t_0}^{*}(\cdot)$ is the fractional integral. If additionally $f \in C[a, b]$ or $m + n \geqslant 1$, then the identity holds everywhere on $[t_0, t]$.

The relationship between the Caputo and Riemann-Liouville differentials is defined as follows.

Lemma 2 (Lemma 3.5 of [34]). Let $\alpha \geqslant 0$ and assume that $f(t), t \in [t_0, T)$ such that ${}_{t_0}^{C}\mathscr{D}_t^{\alpha} f(t)$ and ${}_{t_0}^{\mathrm{RL}}\mathscr{D}_t^{\alpha} f(t)$ exist. Then,

$$ {}_{t_0}^{C}\mathscr{D}_t^{\alpha} f(t) = {}_{t_0}^{\mathrm{RL}}\mathscr{D}_t^{\alpha} [f(t) - f(t_0)] = {}_{t_0}^{\mathrm{RL}}\mathscr{D}_t^{\alpha} f(t) - \frac{f(t_0)}{\Gamma(1-\alpha)} (t - t_0)^{-\alpha}, $$

and ${}_{t_0}^{C}\mathscr{D}_t^{\alpha} f(t) = {}_{t_0}^{\mathrm{RL}}\mathscr{D}_t^{\alpha} f(t)$ holds if and only if $D^k f(t_0) = 0$ for $k = 0, 1, \ldots, m-1$, where ${}_{t_0}^{\mathrm{RL}}\mathscr{D}_t^{\alpha} f(t)$ is the Riemann-Liouville fractional differential with α-order.

The existing commutative law for Caputo fractional derivatives is given in Lemma 3.

Lemma 3 (Lemma 3.13 of [34]). Let f be a function of the derivative of order k, and the derivative is continuous, that is, $f \in C^k[a, b]$ for some $a < b$ and some $k \in \mathbb{N}$. Moreover, let $n, \varepsilon > 0$ such that there exist some $\ell \in \mathbb{N}$ with $\ell \leqslant k$ and $n, n + \varepsilon \in [\ell - 1, \ell]$. Then, ${}_{t_0}^{C}\mathscr{D}_t^{\varepsilon} [{}_{t_0}^{C}\mathscr{D}_t^{n} f(t)] = {}_{t_0}^{C}\mathscr{D}_t^{\varepsilon+n} f(t)$.

Connecting the Caputo operator with a differential operator of the Riemann-Liouville type satisfies the following conclusions.

Lemma 4 (Theorem 3.14 of [34]). Let $f \in C^k[a, b]$ for some $k \in \mathbb{N}$. Moreover, let $n \in [0, k]$. Then, ${}_{t_0}^{\mathrm{RL}}\mathscr{D}_t^{\varepsilon} [{}_{t_0}^{C}\mathscr{D}_t^{n} f(t)] = D^k f(t)$. The operator D^k on the right-hand side of the function is a classical (integer order) differential operator.

Subsequently, we can prove the following commutative law of the Caputo fractional derivative with more general conditions in terms of Lemmas 1–4.

Theorem 1. Let $\varepsilon(t) \in C^k[t_0, t]$, $t_0 < t$ and some $k \in N$.

$$ {}_{t_0}^{C}\mathscr{D}_t^{\alpha}[{}_{t_0}^{C}\mathscr{D}_t^{\beta}\varepsilon(t)] = {}_{t_0}^{C}\mathscr{D}_t^{\beta}[{}_{t_0}^{C}\mathscr{D}_t^{\alpha}\varepsilon(t)] = {}_{t_0}^{C}\mathscr{D}_t^{\alpha+\beta}\varepsilon(t). $$

If $\alpha, \beta > 0$ such that there exist some $l_1, l_2 \in N$ with $l_1, l_2 \leqslant k$ and $\alpha \in (l_1, l_1+1)$, $\beta \in (l_2, l_2+1)$.

Proof. Without loss of generality, $\varepsilon(t_0)$ is the constant value function, which makes the following two conclusions hold: (1) ${}_{t_0}^{C}\mathscr{D}_t^{\beta}\varepsilon(t_0) = 0$, (2) ${}_{t_0}^{C}\mathscr{D}_t^{\alpha}\varepsilon(t_0) = 0$. Based on Lemmas 1 and 2, we derive ${}_{t_0}^{C}\mathscr{D}_t^{\alpha}[{}_{t_0}^{C}\mathscr{D}_t^{\beta}\varepsilon(t)] = \mathscr{D}^{\lceil\alpha\rceil} J_{t_0}^{\lceil\alpha\rceil-\alpha}[J_{t_0}^{\lceil\beta\rceil-\beta}\mathscr{D}^{\lceil\beta\rceil}\varepsilon(t)]$, where $\mathscr{D}^k(\cdot)$, $k = \lceil\alpha\rceil$ or $\lceil\beta\rceil$ is the integer order differentiation. Subsequently, according to Lemma 1, the previously presented equation can be further simplified as follows:

$$ \begin{aligned} {}_{t_0}^{C}\mathscr{D}_t^{\alpha}[{}_{t_0}^{C}\mathscr{D}_t^{\beta}\varepsilon(t)] &= \mathscr{D}^{\lceil\alpha\rceil} J_{t_0}^{\lceil\alpha\rceil-\alpha}[J_{t_0}^{\lceil\beta\rceil-\beta}\mathscr{D}^{\lceil\beta\rceil}\varepsilon(t)] \\ &= J^{-(\lceil\alpha\rceil+\lceil\beta\rceil)} J_{t_0}^{\lceil\alpha\rceil+\lceil\beta\rceil-\alpha-\beta}\varepsilon(t) = D^{(\lceil\alpha\rceil+\lceil\beta\rceil)} J_{t_0}^{\lceil\alpha\rceil+\lceil\beta\rceil-\alpha-\beta}\varepsilon(t). \end{aligned} $$

Similarly,

$$ \begin{aligned} {}_{t_0}^{C}\mathscr{D}_t^{\beta}[{}_{t_0}^{C}\mathscr{D}_t^{\alpha}\varepsilon(t)] &= \mathscr{D}^{(\lceil\beta\rceil+\lceil\alpha\rceil)} J_{t_0}^{\lceil\beta\rceil+\lceil\alpha\rceil-\alpha-\beta}\varepsilon(t) \\ &= J^{-\lceil\beta\rceil} J^{-\lceil\alpha\rceil} J_{t_0}^{\lceil\beta\rceil-\beta} J_{t_0}^{\lceil\alpha\rceil-\alpha} = \mathscr{D}^{(\lceil\alpha\rceil+\lceil\beta\rceil)} J_{t_0}^{\lceil\alpha\rceil+\lceil\beta\rceil-\alpha-\beta}\varepsilon(t). \end{aligned} $$

So far, we have proven that ${}_{t_0}^{C}\mathscr{D}_t^{\alpha}[{}_{t_0}^{C}\mathscr{D}_t^{\beta}\varepsilon(t)] = {}_{t_0}^{C}\mathscr{D}_t^{\beta}[{}_{t_0}^{C}\mathscr{D}_t^{\alpha}\varepsilon(t)] = \mathscr{D}^{(\lceil\alpha\rceil+\lceil\beta\rceil)} J_{t_0}^{\lceil\alpha\rceil+\lceil\beta\rceil-\alpha-\beta}\varepsilon(t)$. According to the conditions, there are $\alpha+\beta \in (l_1+l_2, l_1+l_2+2)$ and $\lceil\alpha\rceil + \lceil\beta\rceil = l_1+l_2+2$. Thus, we consider the following two cases.

Case (1): $\alpha+\beta \in (l_1+l_2, l_1+l_2+1]$. In this case, we derive $\lceil\alpha+\beta\rceil = l_1+l_2+1 = \lceil\alpha\rceil + \lceil\beta\rceil - 1$; hence,

$$ \mathscr{D}^{(\lceil\alpha\rceil+\lceil\beta\rceil)} J_{t_0}^{\lceil\alpha\rceil+\lceil\beta\rceil-\alpha-\beta}\varepsilon(t) = \mathscr{D}^{(\lceil\alpha+\beta\rceil)}\mathscr{D}^1 J^1 J_{t_0}^{\lceil\alpha+\beta\rceil-\alpha-\beta}\varepsilon(t) = \mathscr{D}^{(\lceil\alpha+\beta\rceil)} J_{t_0}^{\lceil\alpha+\beta\rceil-\alpha-\beta}\varepsilon(t) = {}_{t_0}^{C}\mathscr{D}_t^{\alpha+\beta}\varepsilon(t). $$

Case (2): $\alpha+\beta \in (l_1+l_2+1, l_1+l_2+2)$. In this case, we derive $\lceil\alpha+\beta\rceil = l_1+l_2+2 = \lceil\alpha\rceil + \lceil\beta\rceil$; hence,

$$ \mathscr{D}^{(\lceil\alpha\rceil+\lceil\beta\rceil)} J_{t_0}^{\lceil\alpha\rceil+\lceil\beta\rceil-\alpha-\beta}\varepsilon(t) = \mathscr{D}^{(\lceil\alpha+\beta\rceil)} J_{t_0}^{\lceil\alpha+\beta\rceil-\alpha-\beta}\varepsilon(t) = {}_{t_0}^{C}\mathscr{D}_t^{\alpha+\beta}\varepsilon(t). $$

In summary, the calculation of the Caputo fractional differential is commutative, that is, ${}_{t_0}^{C}\mathscr{D}_t^{\alpha}[{}_{t_0}^{C}\mathscr{D}_t^{\beta}\varepsilon(t)] = {}_{t_0}^{C}\mathscr{D}_t^{\beta}[{}_{t_0}^{C}\mathscr{D}_t^{\alpha}\varepsilon(t)] = {}_{t_0}^{C}\mathscr{D}_t^{\alpha+\beta}\varepsilon(t)$.

Then, the following two corollaries can be obtained according to Theorem 1.

Corollary 1. Let $\varepsilon(t) \in C^k[t_0, t]$, $t_0 < t$ and some $k \in N$.

$$ {}_{t_0}^{C}\mathscr{D}_t^{\alpha}[{}_{t_0}^{C}\mathscr{D}_t^{\beta}\varepsilon(t)] = {}_{t_0}^{C}\mathscr{D}_t^{\beta}[{}_{t_0}^{C}\mathscr{D}_t^{\alpha}\varepsilon(t)] = {}_{t_0}^{C}\mathscr{D}_t^{\alpha+\beta}\varepsilon(t). $$

If $\alpha, \beta > 0$ such that there exist some $l \in N$ with $l \leqslant k$ and $\alpha+\beta \in (l, l+1)$.

Corollary 2. Let $\varepsilon(t) \in C^k[t_0, t]$, $t_0 < t$ and some $k \in N$.

$$ {}_{t_0}^{C}\mathscr{D}_t^{\alpha}[{}_{t_0}^{C}\mathscr{D}_t^{\beta}\varepsilon(t)] = {}_{t_0}^{C}\mathscr{D}_t^{\beta}[{}_{t_0}^{C}\mathscr{D}_t^{\alpha}\varepsilon(t)] = {}_{t_0}^{C}\mathscr{D}_t^{\alpha+\beta}\varepsilon(t) $$

holds when $\alpha \in (0,1)$ and $\beta \in (0,1)$.

Remark 1. The conditions in Corollary 1 satisfy $\alpha+\beta \in (l, l+1)$, that is, $\lceil\alpha+\beta\rceil = \lceil\beta\rceil \in (l, l+1)$, and are equivalent to the case where $l_2 = 0$ in Case (1). Then, its proof can be obtained similarly; thus, it will not be repeated.

Remark 2. The conditions in Corollary 2 satisfy $\alpha \in (0,1)$ and $\beta \in (0,1)$ and are equivalent to the case where $l_1 = l_2 = 0$ of Theorem 1. Then, its proof will not be repeated.

Remark 3. The conditions of Theorem 1 are more general than Lemma 3, and its conclusion can cover the conclusion in Lemma 3. Therefore, it has a wider range of applications and more general conclusion.

The variable-order Caputo fractional differentiation is the focus of this study. According to Definition 1, as a direct extension, the Caputo variable-order fractional derivative is defined as follows:

$$ {}_{t_0}^{C}\mathscr{D}_t^{\alpha(t)} f(t) = \frac{1}{\Gamma(n-\alpha(t))} \int_{t_0}^{t} \frac{f^{(n)}(\tau)}{(t-\tau)^{\alpha(t)-n+1}}\, \mathrm{d}\tau, \quad n-1 < \alpha(t) < n. \tag{3} $$

In general, ${}_{t_0}^{C}\mathscr{D}_t^{\alpha(t)} {}_{t_0}^{C}\mathscr{D}_t^{\beta(t)} f(t) \neq {}_{t_0}^{C}\mathscr{D}_t^{\alpha(t)+\beta(t)} f(t)$, even though the weaker form of the index rule (when $\alpha(t)$ and $\beta(t)$ are constants, as shown in Theorem 1) is satisfied under well-defined conditions. For many problems in mechanics, conforming to the weak form of the index rule suffices.

In this research, combined with the actual measurement of asphalt rutting data, cumulative equivalent single axle loads (ESALs) are used to measure the effect of traffic loads. The experience at the end of each load cycle is recorded through the pavement management system and determined based on the uniaxial load, number of load repetitions, and axle and wheel set coefficients. The independent variable t in (3) is the cumulative ESAL. Let E be the set of cumulative ESALs, which is a measurable set. Depending on the loading date of the actual experiment, $\alpha(t)$ is considered a simple function; that is, let us assume that the domain of $\alpha(t)$ defined as E can be divided into a finite number of mutually disjoint measurable sets $E_1, E_2, \ldots, E_s$, $E = \bigcup_{j=1}^{s} E_j$; then, $\alpha(t)$ is equal to a constant α_j on each E_j. Then,

$$ \alpha(t) = \sum_{j=1}^{s} \alpha_j \chi_{E_j(t)}, \quad t \in E, \tag{4} $$

where $\chi_{E_j(t)}$ is the characteristic function that satisfies the following expression:

$$ \chi_{E_j(t)} = \begin{cases} 1, & t \in E_j, \\ 0, & t \notin E_j. \end{cases} $$

In summary, we obtain Theorem 2.

Theorem 2. Let $\varepsilon(t) \in C^k[t_0, t]$, $t_0 < t$ and some $k \in N$. If $\alpha(t)$ is a simple function, then

$$ {}_{t_0}^{C}\mathscr{D}_t^{\alpha(t)} [{}_{t_0}^{C}\mathscr{D}_t^{\beta} \varepsilon(t)] = {}_{t_0}^{C}\mathscr{D}_t^{\beta} [{}_{t_0}^{C}\mathscr{D}_t^{\alpha(t)} \varepsilon(t)] = {}_{t_0}^{C}\mathscr{D}_t^{\alpha(t)+\beta} \varepsilon(t), $$

with $t \in E$, and $\alpha(t), \beta > 0$ such that there exists some $l_1, l_2 \in N$ with $l_1, l_2 \leqslant k$ and $\alpha(t) \in (l_1, l_1+1)$, $\beta \in (l_2, l_2+1)$.

Proof. According to Theorem 1 and the definition of the simple function, when $t \in E_j$, we derive

$$ \begin{aligned} {}_{t_0}^{C}\mathscr{D}_t^{\alpha(t)} [{}_{t_0}^{C}\mathscr{D}_t^{\beta} \varepsilon(t)] &= {}_{t_0}^{C}\mathscr{D}_t^{\alpha_j} [{}_{t_0}^{C}\mathscr{D}_t^{\beta} \varepsilon(t)] = {}_{t_0}^{C}\mathscr{D}_t^{\alpha_j+\beta} \varepsilon(t) \\ &= {}_{t_0}^{C}\mathscr{D}_t^{\beta} [{}_{t_0}^{C}\mathscr{D}_t^{\alpha_j} \varepsilon(t)] = {}_{t_0}^{C}\mathscr{D}_t^{\beta} [{}_{t_0}^{C}\mathscr{D}_t^{\alpha(t)} \varepsilon(t)] = {}_{t_0}^{C}\mathscr{D}_t^{\alpha(t)+\beta} \varepsilon(t). \end{aligned} $$

Set E can be divided into a finite number of mutually disjoint measurable sets $E_1, E_2, \ldots, E_s$ and $E = \bigcup_{j=1}^{s} E_j$. This completes the proof of Theorem 2.

Remark 4. According to the Lusin theorem, $\alpha(t)$ is a finite measurable function nearly everywhere on the domain E; thus, it is a "basically continuous" function. This accurately reflects the test sampling rule of RIOHTrack. Therefore, the continuously varying nature of viscous rheology can be effectively simulated by the fractional variational order.

Remark 5. According to the road test experiment of RIOHTrack, a certain E_j may be a single point set; that is, it can be defined as $E_j = t_j$, $\alpha(t_j) = \alpha_j$. Furthermore, for any $\delta > 0$, there exists $E_\delta = \bigcup_{j=1}^{s_1} E_j$, $s_1 \leqslant s$ such that $\alpha(t)$ in E_δ is a continuous function, $m(E - E_\delta) < \delta$. Notably, $\alpha_j = 0$ is also allowed.

2.2 Laplace transform

In the process of analyzing fractional order systems, the Laplace transform is often used. The following lemma provides the expression of the Laplace transform of the Caputo fractional differential.

Lemma 5 (Chapter 2.8.3 of [35]). The Laplace transform of the Caputo fractional derivative of the function $f(t)$ is expressed as follows:

$$\mathscr{L}\left[{}_0^C\mathscr{D}_t^{\alpha} f(t)\right] = s^{\alpha}F(s) - \sum_{k=0}^{\lceil\alpha\rceil-1} s^{\alpha-k-1}\left[f^{(k)}(t)\right]_{t=0}, \tag{5}$$

where $n-1<\alpha<n$.

According to Lemma 5, the inverse Laplace transform of $s^{-\alpha}$ is expressed as follows:

$$\mathscr{L}^{-1}[s^{-\alpha}] = \frac{t^{\alpha-1}}{\Gamma(\alpha)}. \tag{6}$$

Then, the inverse Laplace transform is performed on $s^{\alpha(t)}$, and the variable-order fractional differential operator suitable for the calculation of the mechanical-empirical model is expressed as follows:

$$\mathscr{L}^{-1}[s^{\alpha(t)}] = \frac{t^{-1-\alpha(t)}}{\Gamma(-\alpha(t))}. \tag{7}$$

The Laplace transform of the two-parameter Mittag-Leffler function is commonly used when applying the Laplace transform to obtain the analytical solution of fractional differential equations, whose definition and transform expression are given as follows.

Definition 2 (Chapter 1.2 in [35]). The two-parameter Mittag-Leffler function is expressed as follows:

$$\Xi_{\alpha,\ \beta}(z) = \sum_{k=0}^{\infty}\frac{z^k}{\Gamma(\alpha k+\beta)}, \tag{8}$$

where $\alpha,\beta\in\mathbb{C}$, $\mathrm{Re}(\alpha)>0$, $\mathrm{Re}(\beta)>0$.

Then, the Laplace transform of a class of generalized Mittag-Leffler functions is defined in Theorem 3.

Theorem 3. Let $k\in\mathbb{R}$ be any real number, and $n<\beta<n-1$; then, the Laplace transform of the following kind of generalized Mittag-Leffler function holds:

$$\mathscr{L}\left\{\frac{t^{\beta+k-1}}{\eta}\Xi_{\beta,\ \beta+k}\left[-\frac{E}{\eta}t^{\beta}\right]\right\} = \frac{1}{s^k(E+\eta s^{\beta})}. \tag{9}$$

Proof. According to the definition of the Laplace transformation and commutative law, then

$$\begin{aligned}\mathscr{L}\left\{\frac{t^{\beta+k-1}}{\eta}\Xi_{\beta,\ \beta+k}\left[-\frac{E}{\eta}t^{\beta}\right]\right\} &= \frac{1}{\eta}\int_0^{+\infty}\mathrm{e}^{-st}t^{\beta+k-1}\sum_{j=0}^{\infty}\frac{[-\frac{E}{\eta}t^{\beta}]^j}{\Gamma(\beta j+\beta+k)}\mathrm{d}t\\ &= \frac{1}{\eta}\sum_{j=0}^{\infty}\frac{[-\frac{E}{\eta}t^{\beta}]^j}{\Gamma(\beta j+\beta+k)}\int_0^{+\infty}\mathrm{e}^{-st}(t)^{\beta+k-1}s\mathrm{d}t.\end{aligned}$$

Multiply the numerator and denominator of the previously presented formula by $s^{(\beta j+\beta+k)}$ to obtain

$$\mathscr{L}\left\{\frac{t^{\beta+k-1}}{\eta}\Xi_{\beta,\ \beta+k}\left[-\frac{E}{\eta}t^{\beta}\right]\right\} = \frac{1}{\eta}\sum_{j=0}^{\infty}\frac{[-\frac{E}{\eta}t^{\beta}]^j s^{-(\beta j+\beta+k)}}{\Gamma(\beta j+\beta+k)}\int_0^{+\infty}\mathrm{e}^{-st}(st)^{\beta j+\beta+k-1}s\mathrm{d}t.$$

Subsequently, let $\zeta=st$, and based on the definition of the Gamma function $\Gamma(z)=\int_0^{+\infty}t^{z-1}\mathrm{e}^{-t}\mathrm{d}t$, $\mathrm{Re}(z)>0$. The following conclusion can be obtained through further calculations:

$$\begin{aligned}\mathscr{L}\left\{\frac{t^{\beta+k-1}}{\eta}\Xi_{\beta,\ \beta+k}\left[-\frac{E}{\eta}t^{\beta}\right]\right\} &= \frac{1}{\eta}\sum_{j=0}^{\infty}\frac{[-\frac{E}{\eta}t^{\beta}]^j s^{-(\beta j+\beta+k)}}{\Gamma(\beta j+\beta+k)}\int_0^{+\infty}\mathrm{e}^{-\zeta}(\zeta)^{\beta j+\beta+k-1}\mathrm{d}\zeta\\ &= \frac{1}{\eta}\sum_{j=0}^{\infty}\frac{[-\frac{E}{\eta}t^{\beta}]^j s^{-(\beta j+\beta+k)}}{\Gamma(\beta j+\beta+k)}\Gamma(\beta j+\beta+k)\\ &= \frac{s^{-k-\beta}}{\eta}\sum_{j=0}^{\infty}\left(-\frac{E}{\eta}\right)^j = \frac{1}{s^k(E+\eta s^{\beta})}.\end{aligned}$$

Theorem 3 is proven.

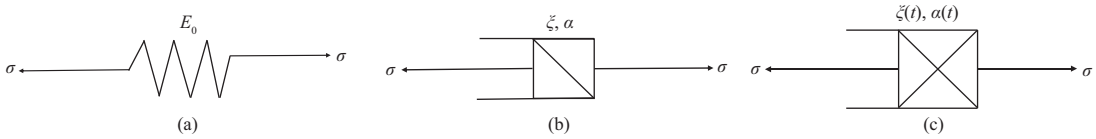

Figure 1 Basic elements. (a) Spring element; (b) Abel sticky pot element; (c) variable-order fractional sticky pot element.

Then, we define Lemma 6 of the inverse Laplace transform of the Mittag-Leffler function of the variable-order fractional derivative. Its proof can be obtained according to Theorems 2 and 3; thus, it is omitted here.

Lemma 6. Let $\alpha(t)$ be a simple function, and $n-1<\beta<n$; then, the Laplace transform of the following kind of generalized Mittag-Leffler function holds:

$$\mathscr{L}\left\{\frac{t^{\beta+\alpha(t)-1}}{\eta}\Xi_{\beta,\ \beta+\alpha(t)}\left[-\frac{E}{\eta}t^{\beta}\right]\right\}=\frac{1}{s^{\alpha(t)}(E+\eta s^{\beta})},\quad t\in E. \tag{10}$$

3 Model establishment

3.1 Basic element

For the classical viscoelastic model, viscoelasticity is usually described in terms of a combination of springs and Newton sticky pots. This is an ideal model where the constitutive relation is proportional to the first derivative of stress and strain. To describe the viscoelastic mechanical behavior of materials more flexibly, Abel constructed sticky pot elements under the fractional differentiation, also known as Abel sticky pot. The constitutive relation of the Abel sticky pot is proportional to the fractional derivatives of stress and strain. To quantitatively describe the time-varying mechanical properties of asphalt mixtures during creep, a nonlinear viscoelastic creep model based on variable-order fractional calculus was proposed. The constitutive relation of the variable-order sticky pot is proportional to the variational derivatives of stress and strain.

For the spring element (see Figure 1(a)), the constitutive relation and creep compliance are given. The constitutive relation of the spring element is expressed as follows:

$$\sigma(t)=E\varepsilon_0(t), \tag{11}$$

where $\sigma(t)$ satisfies $\sigma(t)=\sigma^*H(t)$, σ^* is the constant stress, $H(t)$ is the Heaviside function, $\varepsilon_0(t)$ is the strain of the spring element, and E is the elastic modulus of the spring element MPA. Then, take the Laplace and inverse transforms of the equation to obtain the creep compliance expression of the spring element as

$$J_0(t)=\frac{\sigma^*H(t)}{E}.$$

For the Abel sticky pot element (shown in Figure 1(b)), its constitutive relation equation based on the Caputo fractional differentiation can be expressed as follows:

$$\sigma(t)=\xi\cdot{}_0^C\mathscr{D}_t^{\alpha}\varepsilon_1(t),\quad 0<\alpha<1, \tag{12}$$

where $\varepsilon_1(t)$ is the strain of the Abel dashpot element, $\xi=E_1\tau^{\alpha}$, E_1 is the elastic modulus of the Abel sticky pot, τ is the temperature-dependent average relaxation time, and ${}_0^C\mathscr{D}_t^{\alpha}$ is the Caputo fractional differential operator when $t_0=0$. Notably, when $\alpha\to 0$, the fractional element degenerates into a spring element, and when $\alpha\to 1$, the fractional element degenerates into a Newton sticky pot. Then, the creep compliance $J_1(t)$ of the Abel sticky pot can be obtained through calculations similar to those previously presented, and

$$J_1(t)=\frac{\sigma^*t^{\alpha}}{\xi\Gamma(1+\alpha)}=\frac{\sigma^*}{E_1\Gamma(1+\alpha)}\left(\frac{t}{\tau}\right)^{\alpha}. \tag{13}$$

At the initial stage of loading, the damper element undergoes strain inertia, the gap within the asphalt mixture decreases, and the hardening phenomenon occurs. Therefore, the capability of the road surface to resist deformation gradually increases, and the creep rate gradually decreases. This stage is called

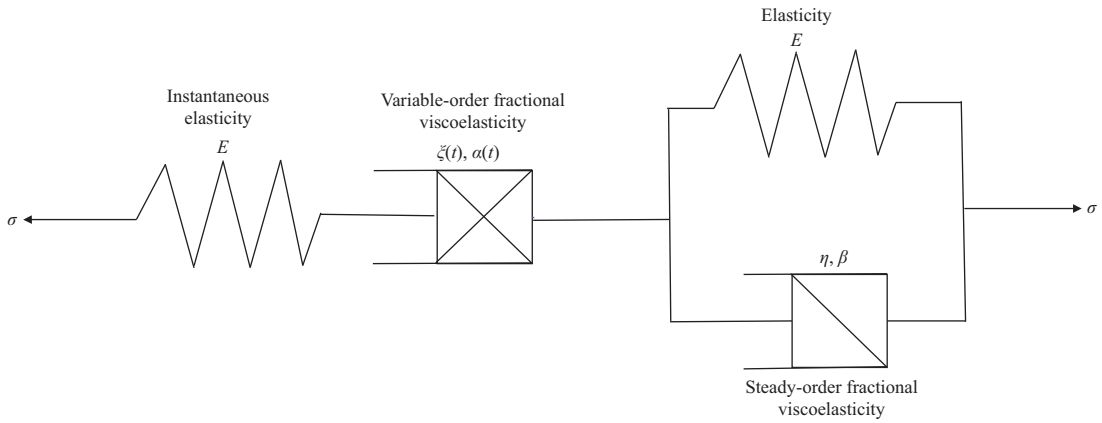

Figure 2 Variable-order fractional derivative Burgers creep model.

the decay creep stage, which is simulated by variable-order fractional viscoelastic elements. Then, for the variable-order sticky pot element (shown in Figure 1(c)), its constitutive relation equation based on variable-order Caputo fractional differentiation can be expressed as follows:

$$\sigma(t) = \xi(t)\,{}_0^C\mathscr{D}_t^{\alpha(t)}\varepsilon_2(t), \tag{14}$$

where $\varepsilon_2(t)$ is the strain of the variable-order fractional sticky pot element, $\xi(t) = E\tau^{\alpha(t)}$, E is the elastic modulus of the variable-order fractional sticky pot, and $\alpha(t)$ is a simple function. The previously presented equation can be rewritten as follows:

$$\sigma(t) = \xi_j(t)\,{}_{t_0}^C\mathscr{D}_t^{\sum_{i=1}^s \alpha_j\chi_{E_j(t)}}\varepsilon_2(t) = E\tau^{\sum_{j=1}^s \alpha_j\chi_{E_j(t)}}\,{}_{t_0}^C\mathscr{D}_{tj}^{\sum_{j=1}^s \alpha_j\chi_{E_j(t)}}\varepsilon_2(t). \tag{15}$$

According to the definition of the simple function, $\xi_j(t) = E\tau^{\alpha_j} = \xi_j$ for $t \in E_j$; then, $\xi(t)$ is a simple function. Then, the creep compliance is calculated as follows:

$$J_2(t) = \frac{\sigma^*}{E\tau^{\alpha(t)}\Gamma[n+\alpha(t)]}t^{\alpha(t)}. \tag{16}$$

3.2 Variable-order fractional Burgers creep model of asphalt pavement

According to existing research, variable-order fractional calculus is an extension of fractional calculus. Theoretically, the change of order can better reflect the evolution of the mechanical properties of asphalt materials. Therefore, this study proposed a creep model based on the Caputo variable-order fractional derivative, as shown in Figure 2.

First, the asphalt mixture will produce a transient elastic deformation independent of the time of loading under the action of constant stress $\sigma(t) = \sigma^* H(t)$, and it is expressed as follows:

$$\varepsilon_0 = \frac{\sigma^*}{E}. \tag{17}$$

In the early stage of loading, the elastic modulus of the asphalt component in the mixture is low, and viscous flow easily occurs. This stage is the decay creep stage. During this period, the material gap and creep rate decrease, as in stage I in Figure 3. After a period of loading, the viscous flow of the variable-order fractional Abel sticky pot element reaches a certain level. At this point, the voids in the asphalt mixture become smaller, and the element still has the possibility of viscous flow, but the stress-bearing elements increase, expanding to all elements in the model. Therefore, the creep rate of the asphalt mixture tends to be stable. This stage is called the steady creep stage in stage II in Figure 3.

Based on (11)–(17) and Theorem 2, through simple calculation, the rheological constitutive equation between strain ε and stress σ of the variable-order fractional Burgers model can be obtained as follows:

$$E\xi(t)\,{}_{0^+}^C\mathscr{D}_t^{\alpha(t)}\varepsilon(t) + \eta\xi(t)\,{}_{0^+}^C\mathscr{D}_t^{\alpha(t)+\beta}\varepsilon(t) = E\sigma(t) + \xi(t)\,{}_{0^+}^C\mathscr{D}_t^{\alpha(t)}\sigma(t) + \eta\,{}_{0^+}^C\mathscr{D}_t^{\beta}\sigma(t), \tag{18}$$

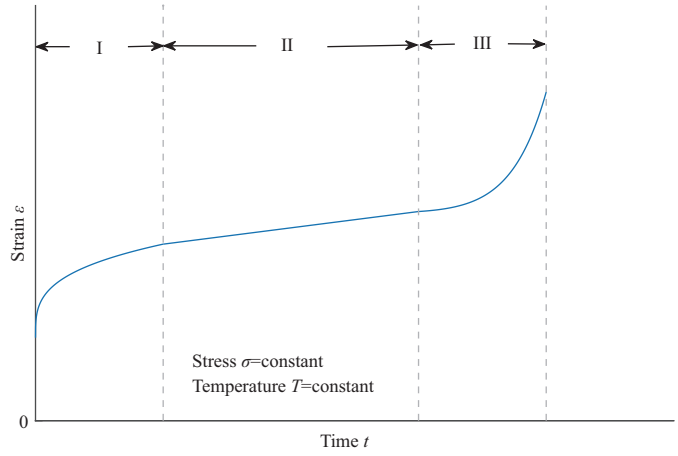

Figure 3 (Color online) Schematic diagram of a typical creep curve.

where $\xi(t)$ and η are the time-varying and constant viscosity coefficients, respectively, and $\alpha(t)$ and β are the variable-order and constant-order fractional exponents, respectively. According to (5), the Laplace transform of formula (18) can be obtained as follows:

$$\begin{aligned}\tilde{\varepsilon}(t) =&\frac{\sigma^*[E+\eta s^{\beta}+\xi(t)s^{\alpha(t)}]}{s[E\xi(t)s^{\alpha(t)}+\eta\xi(t)s^{\alpha(t)+\beta}]}+\frac{[E\xi(t)s^{\alpha(t)-1}+\eta\xi(t)s^{\alpha(t)+\beta-1}]\varepsilon_{0+}}{[E\xi(t)s^{\alpha(t)}+\eta\xi(t)s^{\alpha(t)+\beta}]}\\ =&\frac{\varepsilon_{0+}}{s}+\frac{E\sigma^*}{s^{\alpha(t)+1}\xi(t)(E+\eta s^{\beta})}+\frac{\eta\sigma^*}{s^{\alpha(t)-\beta+1}\xi(t)(E+\eta s^{\beta})}+\frac{\sigma^*}{s(E+\eta s^{\beta})}.\end{aligned}\tag{19}$$

Based on (7) and the conclusion in Theorem 2 and Lemma 6, the inverse Laplace transform of (19) can be used to obtain the creep strain equation of the model as follows:

$$\begin{aligned}\varepsilon(t) =&\mathscr{L}^{-1}[\tilde{\varepsilon}(t)]\\ =&\frac{\sigma^*}{E}+\frac{\sigma^*}{\eta}t^{\beta}\Xi_{\beta,\ \beta+1}\left(-\frac{E}{\eta}t^{\beta}\right)+\frac{\sigma^*}{\xi(t)}t^{\alpha(t)}\Xi_{\beta,\ \alpha(t)+1}\left(-\frac{E}{\eta}t^{\beta}\right)\\ &+\frac{E\sigma^*}{\xi(t)\eta}t^{\alpha(t)+\beta}\Xi_{\beta,\ \alpha(t)+\beta+1}\left(-\frac{E}{\eta}t^{\beta}\right),\quad t\in E_j.\end{aligned}\tag{20}$$

Because of the temperature sensitivity of the asphalt mixture, the elastic modulus E and viscosity coefficient η of the material can be expressed as temperature (T)-related quantities, that is, $\mathrm{e}^{aT}E$, $\mathrm{e}^{bT}\xi(t)$, and $\mathrm{e}^{bT}\eta$ are used to replace E, $\xi(t)$, and η in the creep equation (20), respectively. The loading time t in the creep equation (20) of the fractional-order Burgers model is the repetition times of 100 kN standard axle load, which can be replaced by accumulative ESALs N. Furthermore, because of the large value of N, non-convergence easily occurs in the process of multivariate nonlinear fitting. Therefore, before fitting analysis, N is divided by constant h, where the choice of constant h is not given in advance, nor does it appear as a fitting coefficient. It is the value with the best fitting effect obtained through continuous attempts in the algorithm. Therefore, the corresponding h values of the discussed asphalt pavement may be different. Through the investigation and analysis, the framework of the variable-order fraction Burgers rutting prediction model is constructed as

$$\begin{aligned}\mathrm{RD}=\sigma^*\Bigg[&\frac{1}{\mathrm{e}^{aT}E}+\frac{(N/h)^{\beta}}{\mathrm{e}^{bT}\eta}\Xi_{\beta,\ \beta+1}\left(-\frac{\mathrm{e}^{aT}E}{\mathrm{e}^{bT}\eta}(N/h)^{\beta}\right)+\frac{(N/h)^{\alpha(t)}}{\mathrm{e}^{bT}\xi(t)}\Xi_{\beta,\ \alpha(t)+1}\left(-\frac{\mathrm{e}^{aT}E}{\mathrm{e}^{bT}\eta}(N/h)^{\beta}\right)\\ &+\frac{\mathrm{e}^{aT}E(N/h)^{\alpha(t)+\beta}}{\mathrm{e}^{2bT}\xi(t)\eta}\Xi_{\beta,\ \alpha(t)+\beta+1}\left(-\frac{\mathrm{e}^{aT}E}{\mathrm{e}^{bT}\eta}(N/h)^{\beta}\right)\Bigg],\end{aligned}\tag{21}$$

where RD is the rutting depth of the variable-order fractional derivative Burgers creep model, that is, 0.1 mm, a and b are the model regression coefficients, and $\Xi_{a,\ b}(\cdot)$ is the generalized Mittag-Leffler function. Subsequently, according to the modified Burgers model, the external damper element characterizing the viscous flow and deformation characteristics of the material in the Burgers model is extended to a

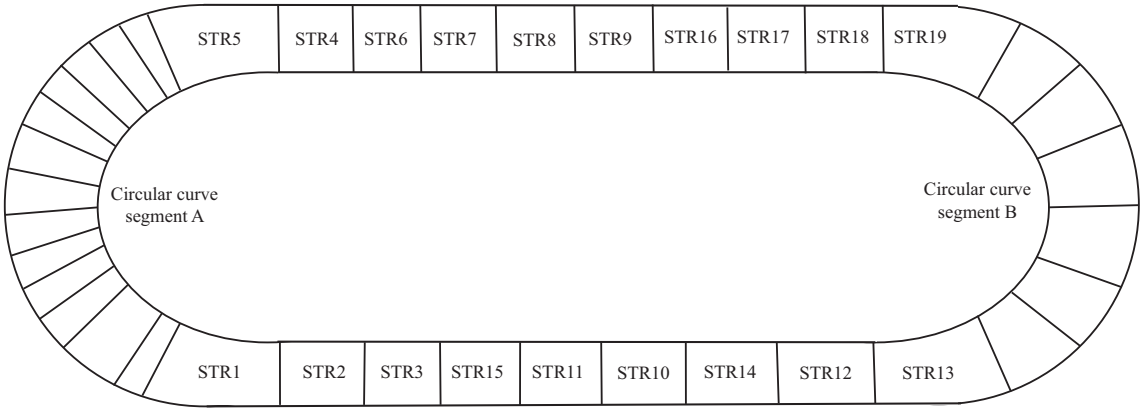

Figure 4 RIOHTrack layout.

generalized damper, and its viscosity is $\xi(t) = A\mathrm{e}^{Bt}$. It can be obtained by simply checking that the order $\alpha(t)$ of the variable-order fractional differential will satisfy the linear form, which can be defined as $\alpha(t) = mt + n$, where m is the order change rate and n is the intercept of $\alpha(t)$ obeying the linear change. Then, Eq. (21) can be rewritten as (22), which is the variable-order fractional Burgers rutting prediction model discussed in this study.

$$\mathrm{RD} = \sigma^* \left[\frac{1}{\mathrm{e}^{aT}E} \frac{(N/h)^{\beta}}{\mathrm{e}^{bT}\eta} \Xi_{\beta,\ \beta+1} \left(-\frac{\mathrm{e}^{aT}E}{\mathrm{e}^{bT}\eta} (N/h)^{\beta} \right) + \frac{(N/h)^{mt+n}}{\mathrm{e}^{bT}A\mathrm{e}^{Bt}} \Xi_{\beta,\ mt+n+1} \left(-\frac{\mathrm{e}^{aT}E}{\mathrm{e}^{bT}\eta} (N/h)^{\beta} \right) + \frac{\mathrm{e}^{aT}E(N/h)^{mt+n+\beta}}{\mathrm{e}^{2bT}A\mathrm{e}^{Bt}\eta} \Xi_{\beta,\ mt+n+\beta+1} \left(-\frac{\mathrm{e}^{aT}E}{\mathrm{e}^{bT}\eta} (N/h)^{\beta} \right) \right]. \tag{22}$$

4 Data collection and analysis

4.1 Pavement materials and structures

The full-scale pavement test track (RIOHTrack) is a close elliptical curve, symmetrically arranged, with a total length of approximately 2039 m and a subgrade width of 15 m, located in China. According to the linear characteristics of the loop and the purpose of the test, the track is divided into 3 parts, and 38 test sections are set up, as shown in Figure 4.

The first part is arranged in the straight track line section and the gentle curve section, with a total length of 1428 m. A total of 19 asphalt pavement structures were laid. The main test pavement structural section is used to assess the long-term performance and evolution of asphalt pavement structures and materials. The second section is arc section A, with a total length of 304.978 m, and 13 sections of cement concrete pavement structure are laid. The third section is section B of the circular curve. Six sections of asphalt pavement structures are laid to assess the anti-rutting technology of asphalt pavement. Among these asphalt pavement structures, according to the structural characteristics of the 19 test pavements, they can be divided into 7 categories. The specific classification methods and descriptions can be found in [30]. The structure of RIOHTrack is shown in Figure 5. Structure I is the semirigid base structure with a strong foundation and a thin surface, which contain three structures, namely, STR1, STR2, and STR3, and the thickness of the asphalt concrete structure layer of these structures is 12 cm. Structure II is a rigid base structure and stress absorption layer, with the structure numbers STR4, STR5, and STR6. Structure III is composed of STR7, STR8, and STR9, which are common asphalt pavement structure forms, and the thickness of the asphalt concrete structure layer for these structures is 18 cm. Structure IV is a combination of asphalt concrete base and semirigid structure, which are STR10 and STR11, respectively. Structure V is a combination of asphalt concrete base and semirigid structure II with an asphalt layer thickness of 24–28 cm, which contains STR12, STR13, and STR14. Structure VI is a combination of asphalt concrete base and semirigid structure III, with the structure numbers STR15, STR16, and STR17. Structure VII is the full-thickness asphalt pavement structure, and the thickness of the asphalt concrete layer reaches 48 cm (STR19) and 52 cm (STR18).

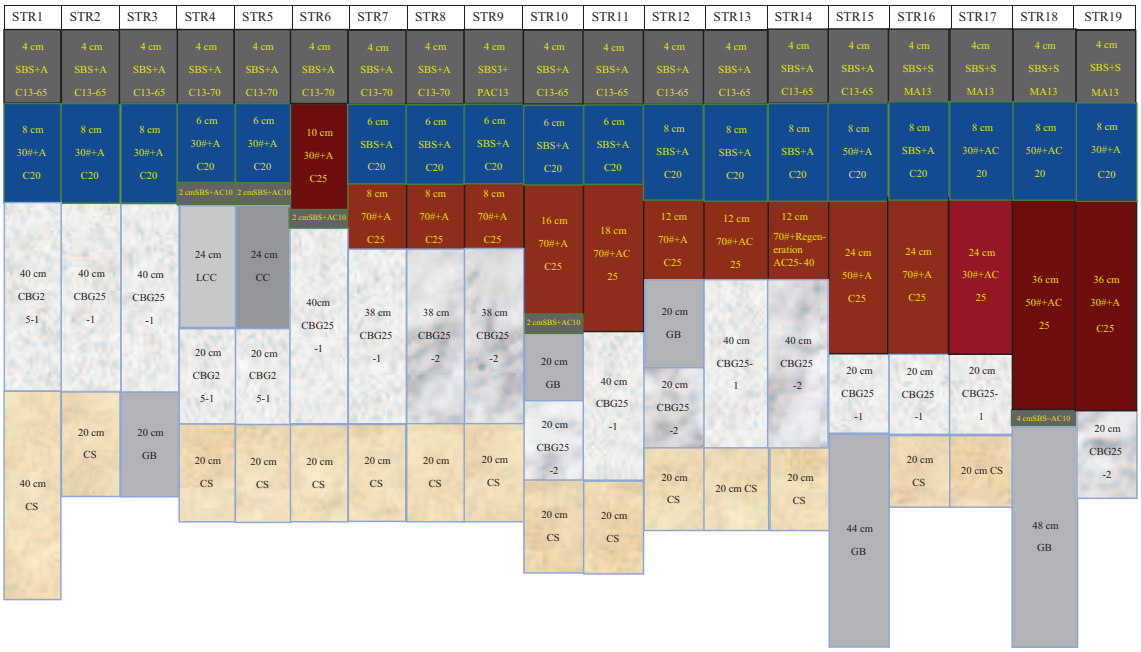

Figure 5 (Color online) RIOHTrack structure.

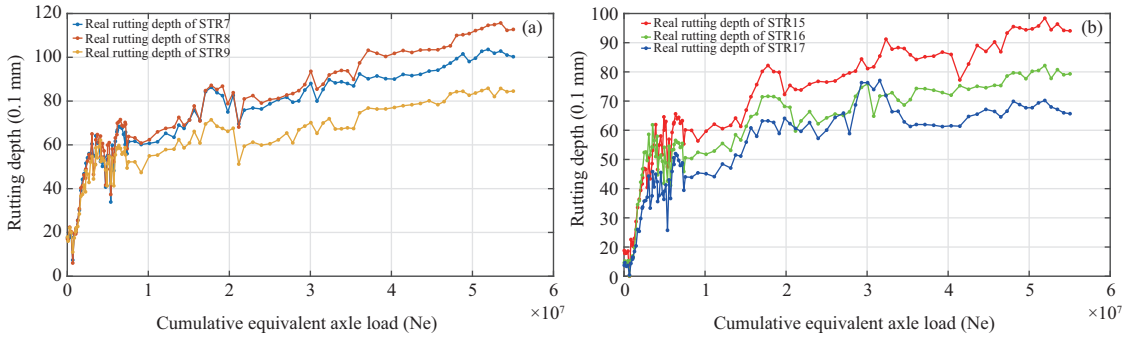

Figure 6 (Color online) Average rutting depth of asphalt pavements in every testing period. (a) STR7, STR8, STR9; (b) STR15, STR16, STR17.

4.2 Rutting depth

The rutting depth is recorded using the customer information control system multifunctional inspection vehicle and measured by the simulated 3-meter-foot method. The maximum rutting depth at the left and right wheelbases is measured, in which the larger one is taken as the rutting depth of the test section. The detection frequency of each test section is 5 m, and the average value is taken as the final rutting depth of each pavement structure. The test method is implemented according to the "RIOHTrack Program Distress Recognition Manual" and the procedures of the asphalt pavement rutting test method (T0973-2008) in the Chinese standard "Highway Engineering Subgrade and Pavement Field Test Methods" (JTG E60-2008) [36]. Manual measurement of depth-of-field rutting is accurate to 0.01 mm. After eliminating the abnormal data, the data were further processed to obtain the average rutting depth of each pavement structure in each test stage. As of November 2021, 5×10^7 loads have been accumulated, and 110 cycles of rutting data have been obtained. Figure 6 shows the rutting data of three kinds of flexible pavement under 110 cycles.

Because of space limitations, this study first discusses structures III and VI as examples. Then, the rutting prediction and comparison results of several representative pavement structures are given to verify that the obtained new rutting prediction model can also accurately predict other road sections of RIOHTrack.

As shown in Figure 6(a), compared with STR8, STR7 has different design strength of the base material. STR7 adopts cement-stabilized graded crushed stone CBG-A with 7d unconfined compressive strength of

6 MPa, and STR8 adopts cement-stabilized graded crushed stone CBG-B with 7d unconfined compressive strength of 4 MPa. The purpose is to verify the relationship between rutting, cracks, water damage, and other diseases of the 18 cm asphalt surface and the strength of the base material. The upper layer of STR9 is made of porous asphalt concrete, and other structures and materials are the same as those of STR8. The durability of the service performance of porous asphalt concrete pavement is discussed mainly from a comprehensive comparison of the surface functional state, structure fatigue resistance, and other aspects [37]. As shown in Figure 6(b), in addition to the SBS-modified asphalt used in the upper layer of STR15, A50 asphalt with smaller penetration is used in the three lower layers. According to the existing indoor test analysis results, its rutting resistance is not less than that of SBS-modified asphalt. STR16 is a commonly used asphalt combination form in the country. The two upper layers use SBS-modified asphalt, and the two lower layers use the commonly used A70 asphalt. Based on STR15, STR17 further reduces the asphalt grade and reaches the A30 standard. In theory, the anti-rutting capability will be further improved. At the same time, the asphalt concrete produced using A30 asphalt belongs to high-modulus asphalt concrete, and the modulus level will be increased by 30%–50% so that the bearing capacity of the pavement structure will also be significantly improved. Because the test track is located in the Tongzhou area of Beijing, the minimum temperature in winter can reach 20°C to 15°C, so the low-temperature crack resistance of this structure needs to be tested [37]. Furthermore, under the same loading times and environmental conditions, the rutting depth of pavement structure STR17 is less than that of pavement structure STR16, which shows that the asphalt concrete produced using A30 asphalt has better rutting resistance than that produced using A70 asphalt. This finding is consistent with the existing research results [38].

5 Model evaluation and comparative analysis

5.1 Model fitting

In this subsection, the mechanical-empirical rutting model is solved by multivariate nonlinear fitting. Multivariate nonlinear fitting is essentially an objective function minimization problem. The optimization methods include gradient descent and Newton's method. The LM algorithm is also a class of methods used to solve the optimal problem of nonlinear least squares multivariate objective functions. The LM algorithm is used in many fields because of its good convergence speed and stability. The LM algorithm is a kind of "trust region method". If the objective function value satisfies certain conditions, then it will be calculated iteratively; if it cannot be satisfied, then the trust region range will be reduced, and the calculation will be repeated until the requirements are met. It is a combination of the gradient descent and the Gauss-Newton method, which can also be considered an improved form of the Gauss-Newton method. The iterative formula of the LM algorithm is expressed as follows:

$$x^{k+1} = x^k - (H + \mu I)^{-1} G, \tag{23}$$

where μ is the step size, G is the first-order gradient of the objective function, and H is the Hessian matrix. When the algorithm drops too rapidly, a smaller μ is used, and the entire formula is close to the Gauss-Newton method. When the algorithm descends too slowly, a larger μ is used, and the entire formula is close to the gradient method. It has both the local convergence of the Gauss-Newton method and the global characteristics of the gradient descent method. Because the LM algorithm utilizes approximate second derivative information, it is much faster than the gradient method.

5.2 Evaluation of the fitting results

In this study, the LM algorithm, as expressed in (23), is used to fit the model, and the regression coefficients $(a, b, m, n, A, B, \beta, \eta, E)$ of the rutting models of STR7, STR8, STR9, STR15, STR16, and STR17 are obtained as shown in Table 1. By substituting the regression coefficients corresponding to the pavement structures in Table 1 into (22), the corresponding mechanical-empirical rutting depth prediction model can be obtained. Here, we omit the obtained formula. Then, the fitting results of three kinds of common asphalt pavement structure forms of structure III are shown in Figure 7, and the fitting results of three kinds of combination forms of structure VI are shown in Figure 8. As shown in Figures 7 and 8 that the rutting depth increases with the increase of loading times, but there will also be periodic changes in the middle. This phenomenon is mainly caused by the change in temperature. When the temperature

Table 1 Regression coefficients (R-C) of the rutting model expressed in (22)

R-C	STR7	STR8	STR9	STR15	STR16	STR17
a	−0.0017	0.0016	0.0042	0.0013	0.0054	0.0030
b	−0.0089	−0.0099	−0.0262	−0.0187	−0.0359	−0.0121
m	10.2902	9.8865	11.5519	8.8564	5.9188	6.7156
n	0.6479	0.4588	0.6399	0.4184	0.5607	0.2736
A	−0.1020	−0.1890	−0.0965	−0.2968	−0.1535	−0.7202
B	−4.3474	−5.8937	−6.1095	−3.1552	11.0535	−5.5480
β	1.1011	1.3836	1.0980	1.0590	0.9333	0.3972
η	5.6321	10.0943	20.5473	8.6325	14.1512	7.4313
E	2.1281	1.6538	1.9144	1.9049	2.0202	2.3008

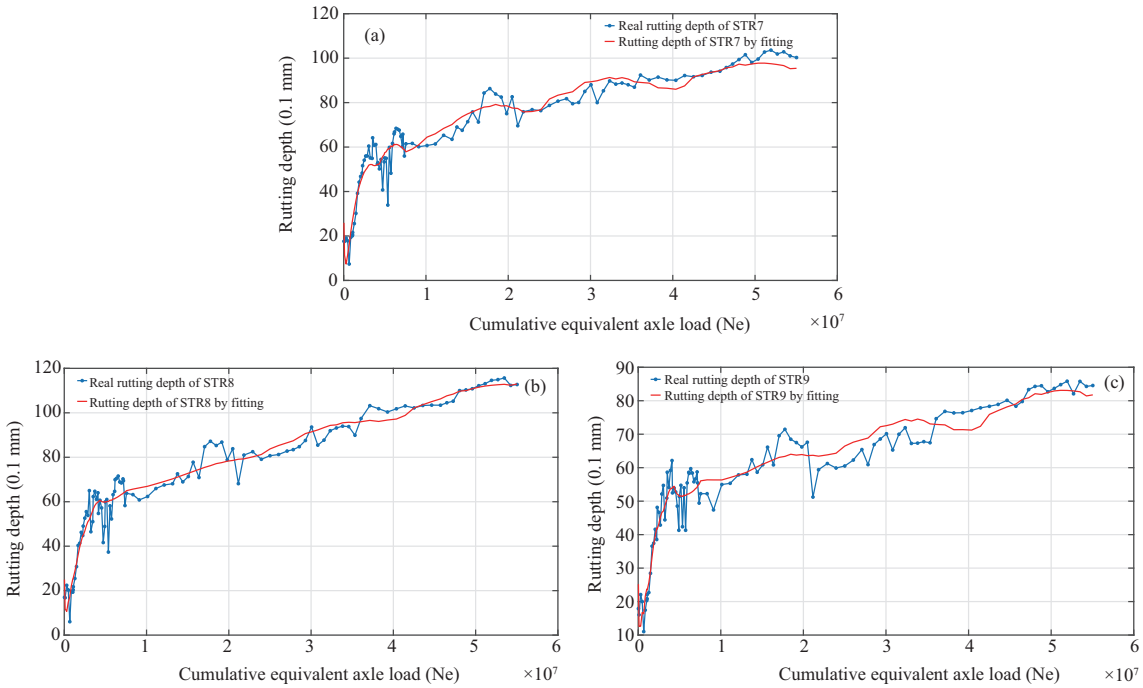

Figure 7 (Color online) Fitting results of the proposed rutting prediction model of three common asphalt pavement structure forms of structure III. (a) STR7; (b) STR8; (c) STR9.

is high in summer, the rutting depth will also increase. Meanwhile, when the temperature decreases, the rutting depth may rebound. Fundamentally, the asphalt mixture is a temperature-sensitive viscoelastic plastic material, and its creep characteristics mainly have an exponential relationship with temperature, which is important for the development of subsequent mechanical-empirical rutting prediction models.

5.3 Comparative analysis with different rutting depth models

In this subsection, the rutting depth prediction model based on the fractional Burgers model proposed in this study is compared with different rutting depth prediction models. The rutting model in [39] is a mechanical-empirical model in the classical mechanistic-empirical pavement design guide (MEPDG) design method, and it can be expressed as follows:

$$\frac{\varepsilon_p}{\varepsilon_r} = aT^b N^c, \tag{24}$$

where ε_p is the accumulated plastic strain after N times of loading, ε_r is the resilient strain, T is the pavement temperature, N is the number of load repetitions, and a, b, and c are the regression coefficients. Then, the LM algorithm is used to fit the model, and the regression coefficients (a, b, c) of the rutting model for different pavement structure types are obtained as shown in Table 2.

Considering the fractional-order Burgers rutting model, that is, letting $\alpha(t) = \alpha_0$ in (18), the creep

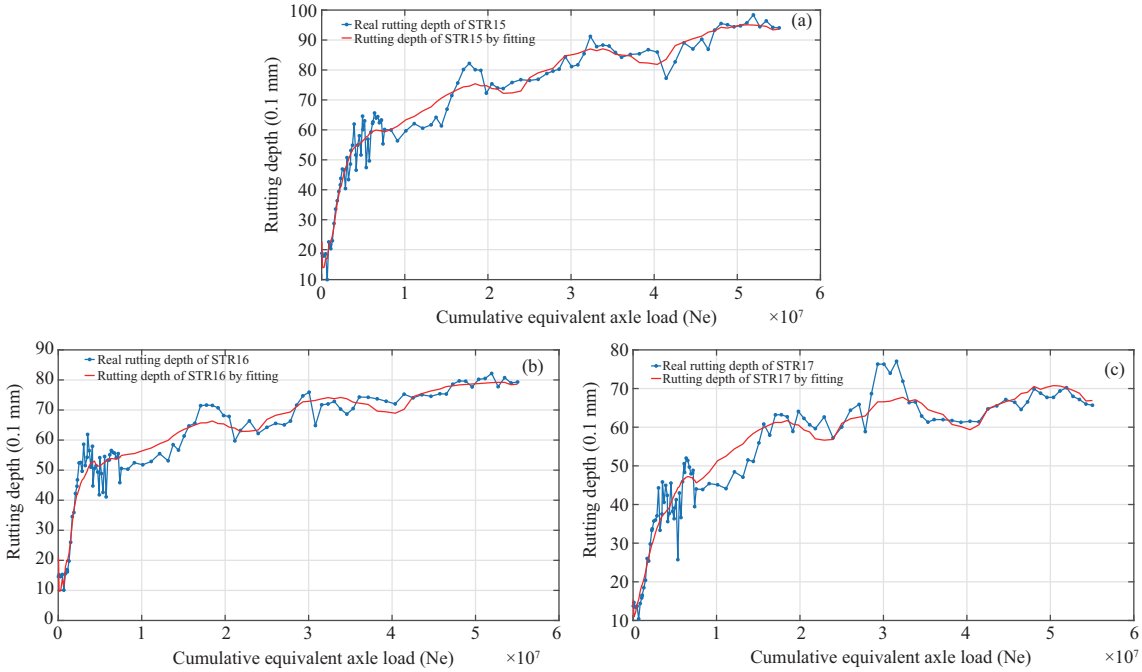

Figure 8 (Color online) Fitting results of the proposed rutting prediction model of three combination forms of structure VI. (a) STR15; (b) STR16; (c) STR17.

Table 2 R-C of the rutting model expressed in (24)

R-C	STR7	STR8	STR9	STR15	STR16	STR17
a	102.45	113.96	84.1882	97.6473	81.9785	73.0667
b	0.26	0.29	0.2251	0.2607	0.2242	0.2525
c	0	0	−0.0012	0.0052	0.0040	0.0101

equation of the fractional Burgers model can be expressed as follows:

$$\varepsilon(t)=\frac{\sigma_0}{E_2}+\frac{\sigma_0}{\eta_2}\frac{t^{\beta}}{\Gamma(\beta+1)}+\frac{\sigma_0}{\eta_1}t^{\alpha_0}\Xi_{\alpha_0,\alpha_0+1}\left(-\frac{E_1}{\eta_1}t^{\alpha_0}\right). \tag{25}$$

Similarly, $\mathrm{e}^{aT}E_1$, $\mathrm{e}^{aT}E_2$, $\mathrm{e}^{bT}\eta_1$, and $\mathrm{e}^{bT}\eta_2$ are used to replace E_1, E_2, η_1, and η_2 in creep equation (25), respectively. Before fitting analysis, N is divided by constant h, where the corresponding h values may be different for different pavement structures. Based on the analysis, the mechanical-empirical model for rutting depth prediction is expressed as follows:

$$\mathrm{RD}=\sigma^*\left[\frac{1}{\mathrm{e}^{aT}E_2}+\frac{1}{\mathrm{e}^{bT}\eta_2}\frac{(\frac{N}{h})^{\beta}}{\Gamma(\beta+1)}+\frac{1}{\mathrm{e}^{bT}\eta_1}\left(\frac{N}{h}\right)^{\alpha_0}\Xi_{\alpha_0,\alpha_0+1}\left(-\frac{\mathrm{e}^{aT}E_1}{\mathrm{e}^{bT}\eta_1}\left(\frac{N}{h}\right)^{\alpha_0}\right)\right], \tag{26}$$

where E_1 and E_2 are the elastic modulus MPA, η_1 and η_2 are the viscosity coefficients, and α and β are the fractional-order exponents. Then, by fitting the model expressed in (26) using the LM algorithm, the regression coefficients $(a, b, E_1, E_2, \eta_1, \eta_2, \alpha_0, \beta)$ of the rutting model for different pavement structure types are obtained as shown in Table 3.

Subsequently, according to [21], the modified Burgers rutting model is expressed as

$$\mathrm{RD}=\sigma^*\left[\frac{1}{\mathrm{e}^{aT}E_2}+\frac{N/h}{\mathrm{e}^{bT}A\mathrm{e}^{Bt}}+\frac{1}{\mathrm{e}^{aT}E_1}\left(1-\mathrm{e}^{-\frac{\mathrm{e}^{aT}E_1}{\mathrm{e}^{bT}\eta_2}(N/h)}\right)\right]. \tag{27}$$

Similarly, the LM algorithm is used to fit the model, and the regression coefficients $(a, b, A, B, E_1, E_2, \eta_2)$ of the rutting model for different pavement structure types are obtained, as shown in Table 4.

Then, the comparison results between the variable-order fractional mechanical-empirical rutting prediction model proposed in this study and the rutting model of MEPDG, fractional-order Burgers rutting

Table 3 R-C of the rutting model expressed in (26)

R-C	STR7	STR8	STR9	STR15	STR16	STR17
a	0.1013	0.0008	0.2022	0.0382	0.0044	−0.0016
b	−0.0148	−0.0039	−0.0034	−0.0172	−0.0088	−0.0071
E_1	0.2718	2.2331	0	2.0641	0.7962	3.8736
E_2	5.8045	3.8461	17.9201	4.0449	9.6206	8.0696
η_1	5.2451	0.3360	1.8437	3.7745	0.7005	3.4396
η_2	1.9415	2.5561	4.9223	1.9990	−0.6259	7.2347
α_0	0.4046	0.9226	0.2180	0.5177	0.4369	0.8491
β	0.2825	0.6742	6.7366	0.3342	3.2046	0.3924

Table 4 R-C of the rutting model expressed in (27)

R-C	STR7	STR8	STR9	STR15	STR16	STR17
a	−0.0018	−0.0022	−0.0045	−0.0023	−0.0013	0.0136
b	−0.0016	0.0039	−0.00148	−0.0008	−0.0022	−0.0254
A	9.25	14.7582	13.5601	10.1405	9.2524	11.2503
B	2.2979	1.9497	2.2480	2.1998	2.7582	3.0804
E_1	0.2877	0.3680	0.1057	0.3639	0.3234	1.0360
E_2	5.5955	11.0319	11.9829	6.8505	6.5559	7.0566
η_2	0.0924	−0.0356	−0.5631	0.0979	0.1732	0.2512

Table 5 Determination coefficients of the rutting depth of types III and VI structures

Model	STR7	STR8	STR9	STR15	STR16	STR17
MEPDG	0.9109	0.9231	0.8650	0.9227	0.8556	0.8800
Fractional-order Burgers model	0.9104	0.9066	0.8750	0.9450	0.8797	0.9110
Modified Burgers model	0.9364	0.9486	0.9263	0.9593	0.9021	0.9391
Rutting model of this paper	0.9404	0.9529	0.9319	0.9702	0.9456	0.9402

model, and modified Burgers rutting model are given. The rutting depth prediction takes the fitting results of structure III, three common asphalt pavement structural forms of asphalt pavement, and structure VI, the combination of asphalt concrete base and semirigid structure III, as examples, as shown in Figures 9 and 10. Figures 9 and 10 show that the rutting prediction models based on different Burgers models can roughly fit the change trend of the real rutting data. Figures 9 and 10 show that the prediction accuracy of the fractional Burgers model with fixed order for rutting on asphalt pavement does not exceed the prediction accuracy of the modified Burgers model. However, when the fixed order is modified to be a variable-order function, the accuracy of rutting prediction of structures III and VI is significantly improved. Based on Table 5, the coefficients of determination R^2 are all greater than 0.93. The predicted values of the rutting models with these structures are close to the measured values. Figures 9 and 10 show that the measured results fluctuate near the prediction curve, and the accuracy is significantly improved.

Subsequently, to further evaluate the three rutting prediction models, we provide the determination coefficient R^2 in Table 5. The theoretical value range of the determination coefficient is $(-\infty, 1]$, and the normal value range is $[0, 1]$. The closer R^2 is to 1, the stronger the explanatory power of the variables of the equation for RD and the better the model fits the data. The closer R^2 is to 0, the worse the model fits. As shown in Table 5, although the rutting model of MEPDG, fractional Burgers rutting depth prediction model, and modified Burgers model fit well, compared with the rutting prediction model of the variable-order fractional Burgers model proposed in this study, the fitting effect is poor. Therefore, the variable-order fractional Burgers mechanics empirical rutting depth prediction model proposed in this study can more accurately predict the rutting depth of these two types of asphalt pavements.

To verify that the new rutting prediction model obtained in this study can also accurately predict other sections in the ring road. Similar to the previously presented discussion, Figure 11 presents a comparison of the results of the rutting models for several representative pavement structures. The results show that, although the existing models can predict rutting, the newly proposed variable-order fractional Burgers rutting prediction model is more accurate, and the predicted value of the rutting model with these structures is closer to the measured value. The measured results fluctuate near the prediction curve, the model prediction error is smaller than the other models, and the prediction accuracy is significantly

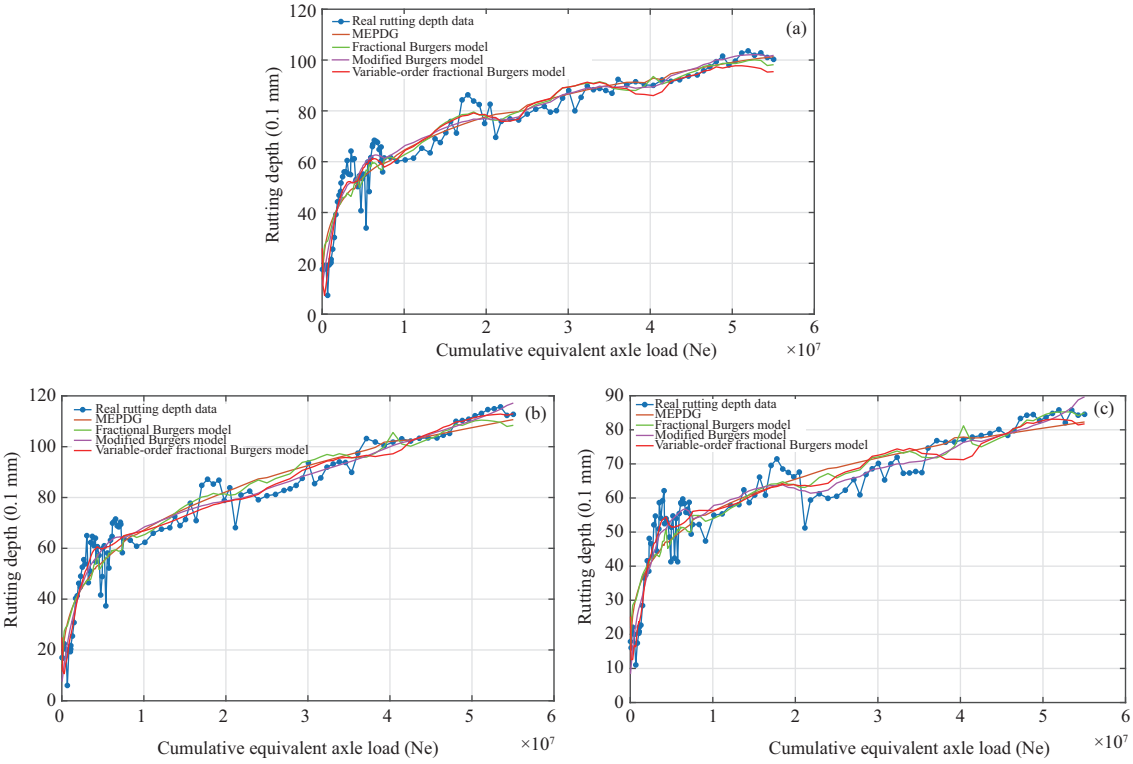

Figure 9 (Color online) Comparison of the prediction performance on three common asphalt pavement structure forms of structure III. (a) STR7; (b) STR8; (c) STR9.

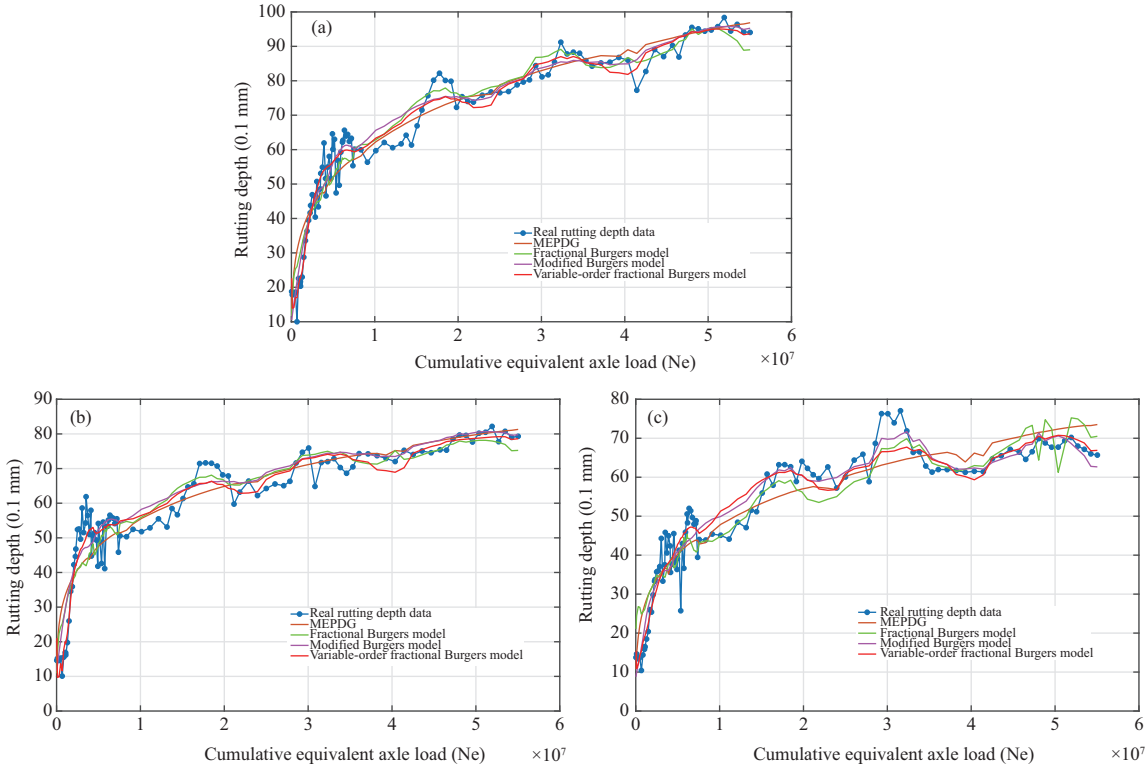

Figure 10 (Color online) Comparison of the prediction performance on three combination forms of structure VI. (a) STR15; (b) STR16; (c) STR17.

improved. In the model prediction, the prediction determination coefficients of different structures are

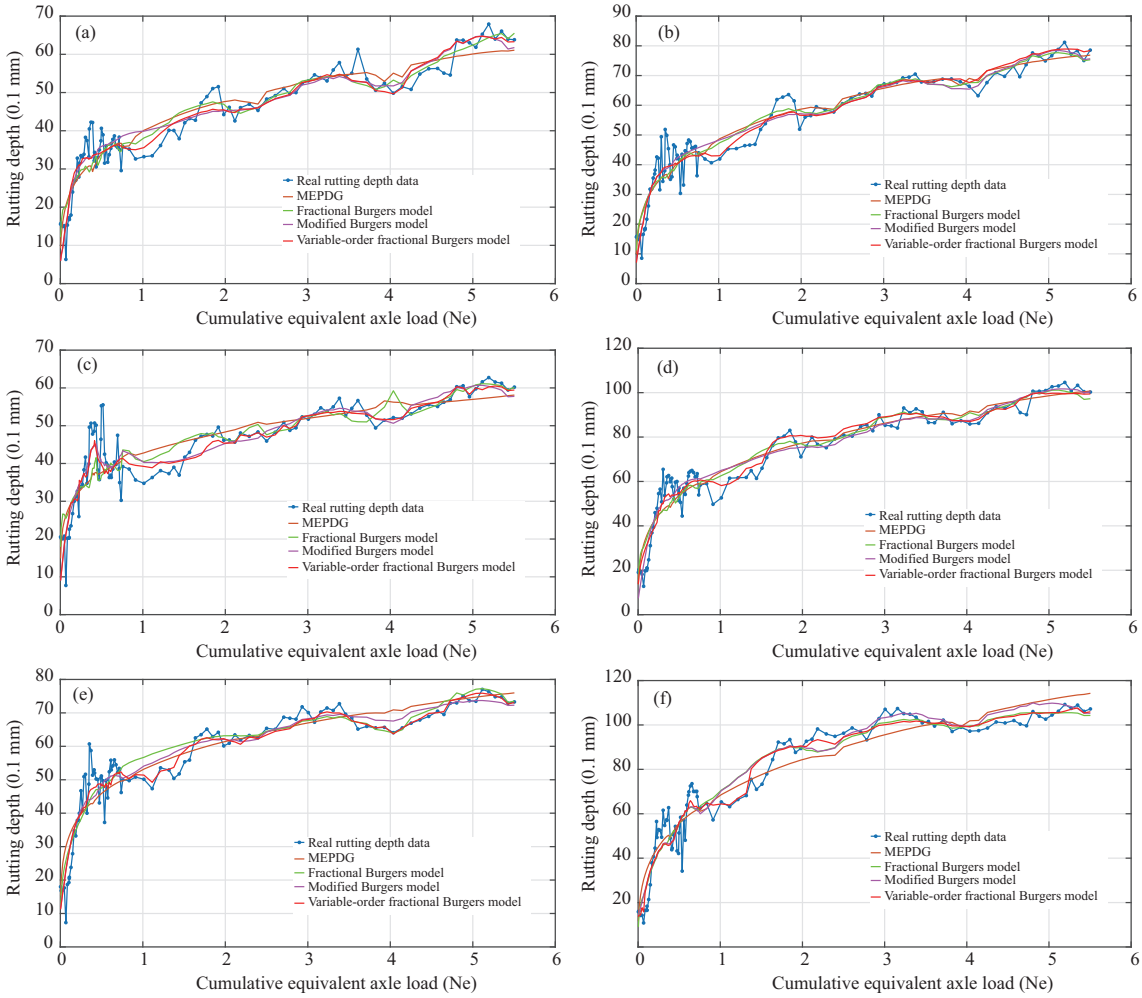

Figure 11 (Color online) Comparison of the results of the rutting models for several representative pavement structures. (a) STR1; (b) STR2; (c) STR5; (d) STR11; (e) STR13; (f) STR18.

Table 6 Coefficients of determination R^2 of several types of pavement structures under different models

Structure type	I	I	II	IV	V	VII
Section number	STR1	STR2	STR5	STR11	STR13	STR18
MEPDG	0.9146	0.9195	0.7567	0.8959	0.8607	0.9132
Fractional-order Burgers model	0.9132	0.9232	0.7794	0.9191	0.8961	0.9382
Modified Burgers model	0.9221	0.9376	0.8565	0.9428	0.9143	0.9372
Rutting model of this paper	0.9315	0.9422	0.8633	0.9507	0.9321	0.9495

obtained, as shown in Table 6. The table shows that the determination coefficient R^2 is greater than 0.86, which indicates that the new variational variable-order Burgers rutting prediction model is suitable for the prediction of various pavement structures in the area located in RIOHTrack.

6 Conclusion

In this study, a mechanical-empirical model for predicting the rutting depth of asphalt pavement structures is established based on the variable-order fractional Burgers model. Compared with the existing rutting prediction models, the model proposed in this study fully considers the influence of the mechanical rheological properties of the asphalt mixture and the temperature on the rutting depth, which well reflects the time-dependent asphalt mixture. The time dependence of the mechanical properties is more pronounced under the action of long-term time series and continuous load. Although the rutting depth prediction model proposed in this study has a good fitting effect on the RIOHTrack full-scale track field

test data, its accuracy and applicability largely depend on the equation form of the model and the empirical coefficients obtained from the data. Therefore, the applicability of the model proposed in this study to asphalt pavement in other fields will be an important research topic in the future. The related work in this research will implement further tracking research and analysis with the update of long-term data rutting. Future work will also further analyze and optimize the model as the RIOHTrack long-term rutting observation data are updated.

Acknowledgements This work was supported in part by National Key Research & Development Project of China (Grant No. 2020YFA0714301) and National Natural Science Foundation of China (Grant No. 61833005).

References

1 Golalipour A, Jamshidi E, Niazi Y, et al. Effect of aggregate gradation on rutting of asphalt pavements. Procedia-Soc Behaval Sci, 2012, 53: 440–449
2 Alae M, Zhao Y, Zarei S, et al. Effects of layer interface conditions on top-down fatigue cracking of asphalt pavements. Int J Pavement Eng, 2020, 21: 280–288
3 Huang W, Liang S M, Wei Y. Surface deflection-based reliability analysis of asphalt pavement design. Sci China Tech Sci, 2020, 63: 1824–1836
4 Ghuzlan K A, Al-Mistarehi B W, Al-Momani A S. Rutting performance of asphalt mixtures with gradations designed using Bailey and conventional Superpave methods. Construction Building Mater, 2020, 261: 119941
5 Luo W, Li B, Zhang Y, et al. A creep model of asphalt mixture based on variable order fractional derivative. Appl Sci, 2020, 10: 3862
6 Barksdale R. Laboratory evaluation of rutting in base course materials. In: Proceedings of the 3rd International Conference on the Structural Design of Asphalt Pavements, London, 1972. 161–174
7 Archilla A R, Madanat S. Development of a pavement rutting model from experimental data. J Transp Eng, 2000, 126: 291–299
8 Darabi M K, Al-Rub R K A, Masad E A, et al. A thermo-viscoelastic-viscoplastic-viscodamage constitutive model for asphaltic materials. Int J Solids Struct, 2011, 48: 191–207
9 Nahi M, Kamaruddin I, Napiah M. Rutting prediction in asphalt pavement based on viscoelastic theory. In: Proceedings of MATEC Web of Conferences, 2016. 78: 01035
10 Al-Rub R K A, Darabi M K, Huang C W, et al. Comparing finite element and constitutive modelling techniques for predicting rutting of asphalt pavements. Int J Pavement Eng, 2012, 13: 322–338
11 Tong J, Ma T, Shen K, et al. A criterion of asphalt pavement rutting based on the thermal-visco-elastic-plastic model. Int J Pavement Eng, 2022, 23: 1134–1144
12 Gong H, Sun Y, Mei Z, et al. Improving accuracy of rutting prediction for mechanistic-empirical pavement design guide with deep neural networks. Construction Building Mater, 2018, 190: 710–718
13 Liu H J, Cao J D, Huang W, et al. Complex network approach for the evaluation of asphalt pavement design and construction: a longitudinal study. Sci China Inf Sci, 2022, 65: 172204
14 Kamboozia N, Ziari H, Behbahani H. Artificial neural networks approach to predicting rut depth of asphalt concrete by using of visco-elastic parameters. Construction Building Mater, 2018, 158: 873–882
15 Mirabdolazimi S M, Shafabakhsh G. Rutting depth prediction of hot mix asphalts modified with forta fiber using artificial neural networks and genetic programming technique. Construction Building Mater, 2017, 148: 666–674
16 Li Z X, Shi X L, Cao J D, et al. CPSO-XGBoost segmented regression model for asphalt pavement deflection basin area prediction. Sci China Tech Sci, 2022, 65: 1470–1481
17 Huang C W, Al-Rub R K A, Masad E A, et al. Three-dimensional simulations of asphalt pavement permanent deformation using a nonlinear viscoelastic and viscoplastic model. J Mater Civ Eng, 2011, 23: 56–68
18 Zhang Y, Luo X, Deng Y, et al. Evaluation of rutting potential of flexible pavement structures using energy-based pseudo variables. Construction Building Mater, 2020, 247: 118391
19 Deng Y, Zhang Y, Shi X, et al. Stress-strain dependent rutting prediction models for multi-layer structures of asphalt mixtures. Int J Pavement Eng, 2022, 23: 2728–2745
20 Chen L, Liu G, Yao B, et al. Rutting prediction model for semirigid base asphalt pavement based on Hamburg wheel tracking test. Int J Geomech, 2021, 21: 04021215
21 Liu G, Chen L, Qian Z, et al. Rutting prediction models for asphalt pavements with different base types based on RIOHTrack full-scale track. Construction Building Mater, 2021, 305: 124793
22 Schapery R A. On the characterization of nonlinear viscoelastic materials. Polym Eng Sci, 1969, 9: 295–310
23 Baglieri O, Santagata E, Sapora A, et al. Fractional viscoelastic modeling of antirutting response of bituminous binders. J Eng Mech, 2017, 143: D4016002
24 Fukunaga M, Shimizu N. Fractional derivative constitutive models for finite deformation of viscoelastic materials. J Comput Nonlinear Dyn, 2015, 10: 061002
25 Celauro C, Fecarotti C, Pirrotta A, et al. Experimental validation of a fractional model for creep/recovery testing of asphalt mixtures. Construction Building Mater, 2012, 36: 458–466
26 Samko S. Fractional integration and differentiation of variable order: an overview. Nonlinear Dyn, 2013, 71: 653–662
27 Wu F, Liu J F, Wang J. An improved Maxwell creep model for rock based on variable-order fractional derivatives. Environ Earth Sci, 2015, 73: 6965–6971
28 Tang H, Wang D, Huang R, et al. A new rock creep model based on variable-order fractional derivatives and continuum damage mechanics. Bull Eng Geol Environ, 2018, 77: 375–383
29 Gao Y, Yin D. A full-stage creep model for rocks based on the variable-order fractional calculus. Appl Math Model, 2021, 95: 435–446
30 Wang X, Zhou G, Liu H, et al. Key points of RIOHTRACK testing road design and construction. J Highway Transp Res Dev (Engl Ed), 2020, 14: 1–16
31 Wu J, Wang X, Wang L, et al. Temperature correction and analysis of pavement skid resistance performance based on RIOHTrack full-scale Track. Coatings, 2020, 10: 832

32 Podlubny I, Chechkin A, Skovranek T, et al. Matrix approach to discrete fractional calculus II: partial fractional differential equations. J Comput Phys, 2009, 228: 3137–3153
33 Caputo M. Linear models of dissipation whose Q is almost frequency independent–II. Geophys J Int, 1967, 13: 529–539
34 Diethelm K. The Analysis of Fractional Differential Equations: An Application-Oriented Exposition Using Operators of Caputo Type. Berlin: Springer, 2004. 55–58
35 Podlubny I. Fractional Differential Equations: An Introduction to Fractional Derivatives. San Diego: Academic Press, 1998. 20–150
36 Ministry of Transport of China. Field Test Methods of Subgrade and Pavement for Highway Engineering (JTG E60-2008). Beijing: China Communications Press, 2008
37 Wang X, Zhou X, Xiao Q, et al. Review of researches of RIOHTrack in 2017 (in Chinese). J Highway Trans Res Dev, 2018, 35: 1–13
38 Li S, Fan M, Xu L, et al. Rutting performance of semi-rigid base pavement in RIOHTrack and laboratory evaluation. Front Mater, 2021, 7: 590604
39 ARA Inc. ERES Consultants Division. Guide for Mechanistic-Empirical Design of New and Rehabilitated Pavement Structures. NCHRP Project 1-37A Final Report, 2004